BIOLOGICAL CRYSTALLOGRAPHY

ISSN 1399-0047

Structural insight into the thermostable NADP$^+$-dependent *meso*-diaminopimelate dehydrogenase from *Ureibacillus thermosphaericus*

Hironaga Akita,[a,b] Tomonari Seto,[c] Toshihisa Ohshima[d] and Haruhiko Sakuraba[e]*

[a]Applied Molecular Microbiology and Biomass Chemistry, Bioscience and Biotechnology, Faculty of Agriculture, Kyushu University, 6-10-1 Hakozaki, Higashi-ku, Fukuoka 812-8581, Japan, [b]Biomass Refinery Research Center, National Institute of Advanced Industrial Sciences and Technology (AIST), 3-11-32 Kagamiyama, Higashi-Hiroshima, Hiroshima 739-0046, Japan, [c]Division of Rare Sugar Science, Faculty of Agriculture, Kagawa University, 2393 Ikenobe, Miki-cho, Kita-gun, Kagawa 761-0795, Japan, [d]Department of Biomedical Engineering, Faculty of Engineering, Osaka Institute of Technology, 5-16-1 Omiya, Asahi-ku, Osaka 535-8585, Japan, and [e]Department of Applied Biological Science, Faculty of Agriculture, Kagawa University, 2393 Ikenobe, Miki-cho, Kita-gun, Kagawa 761-0795, Japan. *Correspondence e-mail: sakuraba@ag.kagawa-u.ac.jp

Received 21 October 2014
Accepted 22 February 2015

Edited by K. Miki, Kyoto University, Japan

Keywords: *meso*-diaminopimelate dehydrogenase; *Ureibacillus thermosphaericus*.

PDB references: *meso*-diaminopimelate dehydrogenase, 3wyb; complex with NADP, 3wyc

Supporting information: this article has supporting information at journals.iucr.org/d

Crystal structures of the thermostable *meso*-diaminopimelate dehydrogenase (DAPDH) from *Ureibacillus thermosphaericus* were determined for the enzyme in the apo form and in complex with NADP$^+$ and *N*-tris(hydroxymethyl)methyl-2-aminoethanesulfonic acid. The main-chain coordinates of the enzyme showed notable similarity to those of *Symbiobacterium thermophilum* DAPDH. However, the subunit arrangement of *U. thermosphaericus* DAPDH (a dimer) was totally different from that of the *S. thermophilum* enzyme (a hexamer). Structural comparison with the dimeric enzyme from the mesophile *Corynebacterium glutamicum* revealed that the presence of large numbers of intrasubunit and intersubunit hydrophobic interactions, as well as the extensive formation of intersubunit ion-pair networks, were likely to be the main factors contributing to the higher thermostability of *U. thermosphaericus* DAPDH. This differs from *S. thermophilum* DAPDH, within which the unique hexameric assembly is likely to be responsible for its high thermostability. Analysis of the active site of *U. thermosphaericus* DAPDH revealed the key factors responsible for the marked difference in substrate specificity between DAPDH and the D-amino acid dehydrogenase recently created from DAPDH by introducing five point mutations [Akita *et al.* (2012). *Biotechnol. Lett.* **34**, 1693–1699; 1701–1702].

1. Introduction

meso-Diaminopimelate dehydrogenase (DAPDH; EC 1.4.1.16) catalyzes the reversible NADP$^+$-dependent oxidative deamination of *meso*-diaminopimelate (*meso*-DAP) to produce L-2-amino-6-oxopimelate within cells (Fig. 1). DAPDH was first identified in *Bacillus sphaericus* (Misono *et al.*, 1979) and has been found to function in L-lysine biosynthesis in both *B. sphaericus* (Misono & Soda, 1980) and *Corynebacterium glutamicum* (Misono *et al.*, 1986). The enzyme is the only known NAD(P)$^+$-dependent dehydrogenase that acts stereoselectively on the D-centre of *meso*-DAP, and it may be useful for the one-step production of D-amino acids, which are often utilized as source materials for the industrial production of medicines, seasonings and agrochemicals. However, the reaction catalyzed by this enzyme is irreversible *in vitro* because the L-2-amino-6-oxopimelate produced from *meso*-DAP is cyclized. In addition, the high substrate specificity for *meso*-DAP has thus far precluded the use of DAPDH in the practical application of D-amino acid

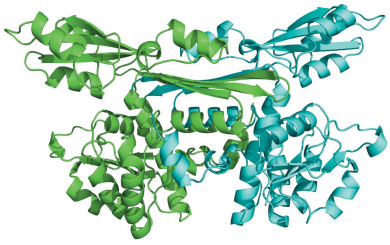

synthesis. Vedha-Peters *et al.* (2006) used error-prone PCR and site-directed mutagenesis to create a novel $NADP^+$-dependent D-amino acid dehydrogenase (DAADH) from *C. glutamicum* DAPDH. This enzyme could be used for the stereoselective synthesis of D-amino acids from the corresponding 2-oxo acids and ammonia in the presence of NADPH. However, because the parent enzyme from mesophilic *C. glutamicum* is rather unstable, this DAADH is not sufficiently stable for use under the conditions necessary for industrial application.

We recently identified and characterized a highly stable DAPDH from the thermophilic bacterium *Ureibacillus thermosphaericus* (Akita *et al.*, 2011). This enzyme showed no loss of activity after incubation for 30 min at temperatures of up to 333 K. Moreover, by introducing five point mutations into amino-acid residues located around the active site, as in the case of the *C. glutamicum* enzyme, we have already succeeded in creating a stable DAADH from *U. thermosphaericus* DAPDH (Akita *et al.*, 2012*a*,*b*). We have also developed novel production methods for D-branched-chain amino acids, for labelling the compounds with stable isotopes (Akita, Suzuki *et al.*, 2014) and for assaying D-isoleucine without interference from the three other isomers (Akita, Imaizumi *et al.*, 2014). More recently, an alternative thermostable DAPDH with a more relaxed substrate specificity was isolated from the uncultivatable thermophilic bacterium *Symbiobacterium thermophilum* (Gao *et al.*, 2012). Gao and coworkers have also constructed a stable DAADH from *S. thermophilum* DAPDH using site-saturation mutagenesis (Gao *et al.*, 2013).

To date, three-dimensional structures of the DAPDH–$NADP^+$ binary complex (Scapin *et al.*, 1996), the DAPDH–*meso*-DAP binary complex (Scapin *et al.*, 1998), a DAPDH–$NADP^+$–inhibitor ternary complex (Scapin *et al.*, 1998) and a DAPDH–NADPH–inhibitor ternary complex (Cirilli *et al.*, 2000) have been solved for the mesophilic *C. glutamicum* enzyme. In addition, structures of *S. thermophilum* DAPDH in its apo form, in complex with $NADP^+$ and in complex with both NADPH and *meso*-DAP have been determined (Liu *et al.*, 2014). Although extensive analysis of these structures has shed light on the structure of the substrate-binding site and has enabled the elucidation of the substrate-recognition mechanism of these enzymes, the structural features responsible for the high thermostability of thermophilic DAPDHs have not yet been determined. Given that the subunit assembly of *S. thermophilum* DAPDH (a hexamer) is quite different from that of *U. thermosphaericus* DAPDH (a dimer), we suggest that the molecular strategy for increasing the thermostability differs between the two enzymes. To test this idea, in the present study, the crystal structure of *U. thermosphaericus* DAPDH was determined. Through comparison with the structure of *C. glutamicum* DAPDH, we then evaluated the structural features responsible for the high thermostability of *U. thermosphaericus* DAPDH and *S. thermophilum* DAPDH. Furthermore, the factors underlying the dramatic change in substrate recognition from DAPDH to DAADH caused by introducing five point mutations were analyzed based on the active-site architecture of *U. thermosphaericus* DAPDH. We anticipate that this structural analysis will provide useful information for the creation of a DAADH mutant exhibiting different coenzyme and substrate specificities and greater stability.

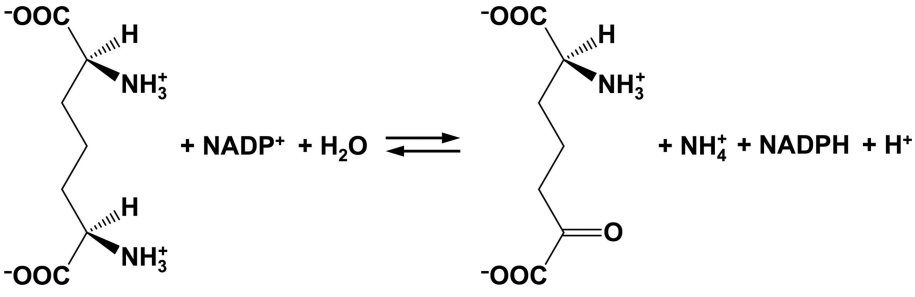

Figure 1
Reaction catalyzed by DAPDH.

2. Materials and methods

2.1. Protein expression and purification

The expression vector (pET-21a/DAPDH) for C-terminal His-tagged DAPDH was constructed as described previously (Akita *et al.*, 2012*a*,*b*). *Escherichia coli* Rosetta (DE3) cells harbouring pET-21a/DAPDH were cultivated for 3 h at 310 K in Luria–Bertani medium (2 l) containing 100 mg l^{-1} ampicillin. Expression was then induced by adding isopropyl β-D-1-thiogalactopyranoside to a final concentration of 1.0 m*M*, after which cultivation was continued for an additional 3 h at 310 K. The cells were then harvested by centrifugation, suspended in 20 m*M* Tris–HCl buffer pH 7.9 containing 500 m*M* NaCl (buffer *A*) and disrupted by ultrasonication. The resulting lysate was heated for 30 min at 328 K and the denatured proteins were removed by centrifugation (27 500*g* for 15 min at 277 K). The supernatant from this step was loaded onto a Ni^+-charged Chelating Sepharose Fast Flow column (20 ml; GE Healthcare, Buckinghamshire, England) equilibrated with buffer *A*. After washing the column with buffer *A* containing 1 m*M* imidazole (40 ml) followed by buffer *A* containing 2 m*M* imidazole (80 ml), the enzyme was eluted with buffer *A* containing 500 m*M* imidazole. The active fractions were pooled and loaded onto a TOYOPEARL Butyl-650M column (40 ml; Tosoh, Tokyo, Japan) equilibrated with buffer *A* and the column was washed with the same buffer. The enzyme was eluted without adsorption, and the active fractions were pooled and dialyzed against 50 m*M* potassium phosphate buffer pH 7.2 (buffer *B*). The dialysate was then applied onto a TOYOPEARL DEAE-650M column (50 ml; Tosoh) equilibrated with buffer *B*. After washing the column with the same buffer, the enzyme was eluted with a linear gradient of 0–0.5 *M* NaCl in buffer *B*. The active fractions were

Table 1
Data-collection and refinement statistics for *U. thermosphaericus* DAPDH.

Values in parentheses are for the highest resolution data shell.

	Apo DAPDH (PDB entry 3wyb)	$NADP^+$/TES-bound DAPDH (PDB entry 3wyc)
Data collection		
Wavelength (Å)	1.0	1.0
Space group	*H*3	*H*3
Unit-cell parameters		
a, *b* (Å)	121.8	123.0
c (Å)	194.1	193.3
α, *β* (°)	90	90
γ (°)	120	120
Resolution range (Å)	50–2.40 (2.44–2.40)	50–2.07 (2.14–2.07)
Total No. of reflections	237733	373429
No. of unique reflections	41892	66282
Multiplicity	5.7 (5.6)	5.6 (5.7)
Completeness (%)	99.9 (100)	99.9 (100)
R_{merge}†	0.072 (0.308)	0.084 (0.296)
$\langle I/\sigma(I)\rangle$	17.4 (8.0)	14.8 (8.2)
Refinement		
Resolution range (Å)	30.8–2.40	31.1–2.07
R/R_{free}‡ (%)	17.3/21.5 (26.1/32.3)	17.3/20.8 (21.6/27.6)
No. of protein atoms	5096	5084
No. of water molecules	198	387
No. of ligands	—	4 TES, 2 $NADP^+$
Average *B* factor (Å^2)	47.0	34.4
R.m.s.d.		
Bond lengths (Å)	0.019	0.022
Bond angles (°)	2.0	2.1
Ramachandran statistics (%)		
Favoured	98.2	98.5
Allowed	1.8	1.5
Outliers	0	0

† $R_{merge} = \sum_{hkl}\sum_i |I_i(hkl) - \langle I(hkl)\rangle| / \sum_{hkl}\sum_i I_i(hkl)$, where $I_i(hkl)$ is the scaled intensity of the *i*th observation of reflection *hkl* and $\langle I(hkl)\rangle$ is the mean value with summation over all measurements. ‡ R_{free} was calculated with randomly selected reflections (5%).

pooled and dialyzed against 10 m*M* potassium phosphate buffer pH 7.2. The entire procedure was carried out at room temperature.

The protein concentration was determined using the method of Bradford (1976) using bovine serum albumin as the standard.

2.2. Crystallization and data collection

For the crystallization of apo DAPDH, purified His-tagged DAPDH in 10 m*M* potassium phosphate buffer pH 7.2 was concentrated to 46.4 mg ml^{-1} by ultrafiltration (Amicon Ultra 30K NMWL; Millipore, Massachusetts, USA). Crystallization was then performed using the sitting-drop vapour-diffusion method, in which 1 µl protein solution was mixed with an equal volume of reservoir solution (1.9 *M* ammonium sulfate, 0.1 *M* Tris–HCl pH 7.5). Crystals of $NADP^+$-bound DAPDH were grown in sitting drops composed of 1 µl enzyme solution (13.2 mg ml^{-1}) containing 1 m*M* $NADP^+$ and 3 m*M* D-lysine mixed with an equal volume of mother liquor composed of 1.9 *M* trisodium citrate dihydrate and 0.1 *M* *N*-tris(hydroxymethyl)methyl-2-aminoethanesulfonic acid (TES) buffer pH 7.5. In all cases, diffraction-quality crystals appeared after 3 d at 293 K.

Diffraction data were collected using an ADSC Quantum CCD detector system on the AR-NW12 and AR-NE3A beamlines at the Photon Factory, Tsukuba, Japan using monochromated radiation at a wavelength of 1.0 Å. All measurements were carried out on crystals cryoprotected with Paratone-N (100%; Hampton Research, Aliso Viejo, California, USA) and cooled to 100 K in a stream of nitrogen gas. The data were processed using *HKL*-2000 (Otwinowski & Minor, 1997).

2.3. Phasing, refinement and structural analysis

The structure of apo DAPDH was solved to a resolution of 2.4 Å by molecular replacement using *MOLREP* (Vagin & Teplyakov, 2010) in the *CCP*4 suite (Winn *et al.*, 2011); the structure of chain *A* of *C. glutamicum* DAPDH (PDB entry 1dap; Scapin *et al.*, 1996) served as the search model. Data in the resolution range 50–3 Å were used in the molecular replacement. *DM* (Cowtan & Main, 1996) was used for noncrystallographic symmetry (NCS) averaging and solvent flattening of the electron-density map (as implemented in the

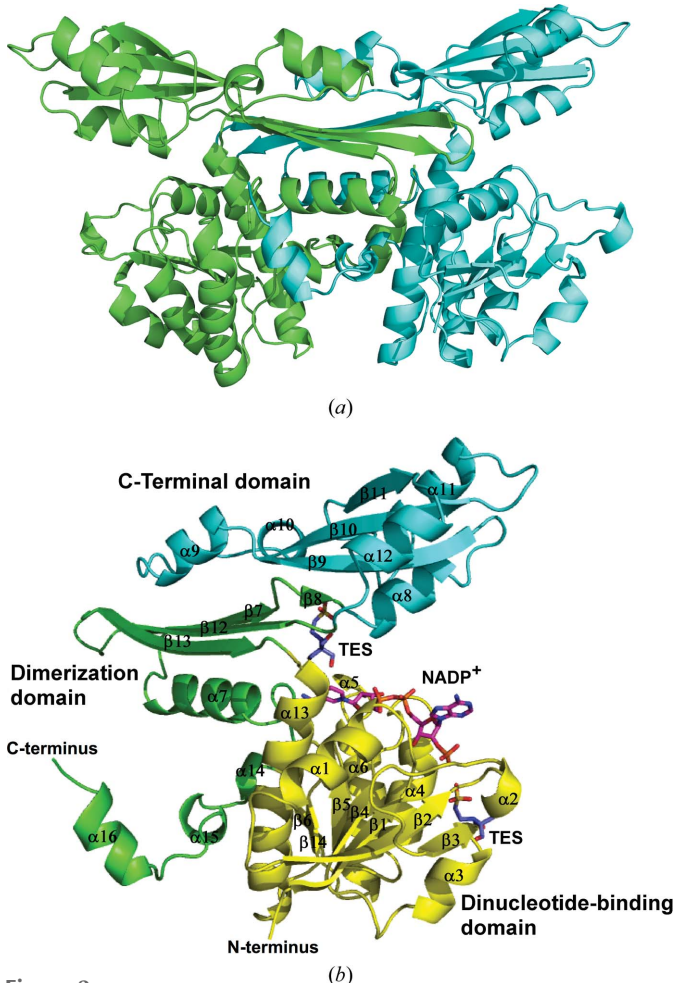

Figure 2
Dimer (*a*) and monomer (*b*) structures of *U. thermosphaericus* DAPDH. (*a*) Subunits *A* and *B* are shown in green and cyan, respectively. (*b*) The dinucleotide-binding domain, the dimerization domain and the C-terminal domain are shown in yellow, green and cyan, respectively. $NADP^+$ and TES molecules are shown in magenta and blue, respectively.

*CCP*4 program *NCSREF*). Model building was performed using *Coot* (Emsley *et al.*, 2010). Maximum-likelihood refinement at 2.4 Å resolution was performed using *REFMAC*5 (Murshudov *et al.*, 2011). NCS restraints were imposed during initial refinement. Simulated-annealing, energy-minimization and *B*-factor refinement were performed using *CNS* (Brünger *et al.*, 1998). After several cycles of inspection of the $2F_o - F_c$ and $F_o - F_c$ density maps, the model was rebuilt. In the final refined model R = 0.173 (R_{free} = 0.215). The structure of $NADP^+$-bound DAPDH was solved to a resolution of 2.07 Å by molecular replacement using *MOLREP* (Vagin & Teplyakov, 2010) with the apoenzyme structure as the search model. The model was rebuilt using *Coot* (Emsley *et al.*, 2010) and refinement at 2.07 Å resolution was performed as described for apo DAPDH. In the final model R = 0.173 (R_{free} = 0.208). In all cases, water molecules were incorporated using *Coot* (Emsley *et al.*, 2010) and model geometry was analyzed using *RAMPAGE* (Lovell *et al.*, 2003). The data-collection and refinement statistics are listed in Table 1.

Ion pairs, with a cutoff distance of 4.0 Å, were identified using the *WHAT IF* (Rodriguez *et al.*, 1998) and *PISA* (Krissinel & Henrick, 2007) web servers. To determine the number of hydrophobic interactions, the interatomic contacts between atoms from hydrophobic side chains were calculated using the *WHAT IF* web server (Rodriguez *et al.*, 1998). A contact was defined as two atoms for which the distance between the van der Waals surfaces was less than 1.0 Å. Hydrogen bonds were identified using *CCP*4*mg* (McNicholas *et al.*, 2011). Accessible surface areas (ASAs; the radius of the probe solvent molecule was 1.4 Å) of the protein and each surface amino-acid residue (charged, Asp, Arg, Glu and Lys; polar, Asn, Cys, Gln, His, Ser, Thr and Tyr; hydrophobic, Ala, Gly, Ile, Leu, Met, Phe, Pro, Trp and Val) were calculated using *AREAIMOL* in the *CCP*4 suite (Winn *et al.*, 2011). Molecular graphics figures were created using *PyMOL* (http://www.pymol.org/).

2.4. Fluorescence-based thermal shift assay

The fluorescence-based thermal shift assay was carried out with a CFX96 Real-Time PCR System (Bio-Rad, Richmond, California, USA) using 470 ± 20 nm excitation and 570 ± 10 nm emission filters in a 96-well plate format (Lo *et al.*, 2004; Watanabe *et al.*, 2014). DAPDH was prepared at a final concentration of 0.1 mg ml^{-1} in 10 m*M* potassium phosphate buffer pH 7.2. After SYPRO Orange dye (Invitrogen, Carlsbad, California, USA) had been added at a 20-fold dilution to the enzyme (total volume 20 µl), the fluorescence intensity was measured at temperatures ranging from 298 to 363 K using a stepwise gradient of 0.1 K s^{-1}. The data were fitted to the Boltzmann equation and the melting temperature (T_m) was calculated using the *Bio-Rad CFX Manager* software (Bio-Rad).

3. Results and discussion

3.1. Overall structure and structural homologues

The structure of apo DAPDH (PDB entry 3wyb) was determined using molecular replacement and was refined at a resolution of 2.4 Å (Table 1). The *U. thermosphaericus* DAPDH protein assembled as a dimer (Fig. 2*a*), which coincided with the subunit assembly of the enzyme in solution (Akita *et al.*, 2011). The asymmetric unit consisted of a single homodimer with a solvent content of 68.0%, which corresponded to a Matthews coefficient (Matthews, 1968) of

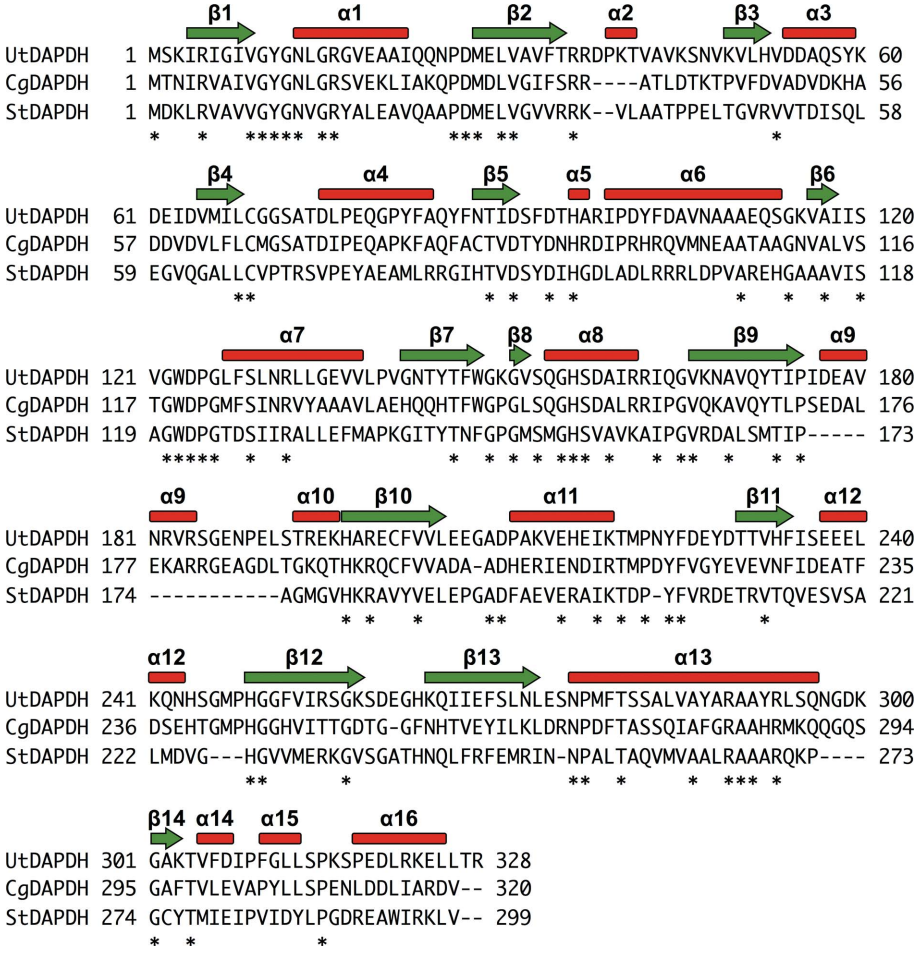

Figure 3
Amino-acid sequences of *U. thermosphaericus* DAPDH (UtDAPDH), *C. glutamicum* DAPDH (CgDAPDH) and *S. thermophilum* DAPDH (StDAPDH). The sequences were aligned using *ClustalW* (Thompson *et al.*, 1994). The secondary-structural assignments for UtDAPDH are shown above the alignment. Conserved residues are indicated with asterisks.

3.9 Å^3 Da^{-1}. The model of the dimer (Fig. 2*a*) contained ordered residues 2–328 (residues 327–328 are part of the C-terminal tag) in each subunit and 198 water molecules. The two molecules in the asymmetric unit were related by a twofold noncrystallographic rotation axis. Each monomer consisted of three domains: a dinucleotide-binding domain (residues 2–120 and 275–304), a dimerization domain (residues 121–152, 247–274 and 305–328) and a C-terminal domain (residues 153–246) (Fig. 2*b*).

When the model of the apo DAPDH monomer was sent to the *DALI* server (Holm & Rosenström, 2010) for the identification of proteins with similar structures (as of 1 August 2014), the protein with the highest structural similarity was *C. glutamicum* DAPDH (PDB entries 1f06, 1dap, 2dap and 3dap; r.m.s.d.s between 1.7 and 2.7 Å; Cirilli *et al.*, 2000; Scapin *et al.*, 1996, 1998), as expected. The *U. thermosphaericus* DAPDH monomer possesses a secondary/tertiary structure resembling that of *C. glutamicum* DAPDH: helices α1–α6 and α13 and β-strands β1–β6 and β14 make up the dinucleotide-binding domain, helices α7 and α14–α16 and β-strands β7, β8, β12 and β13 comprise the dimerization domain and helices α8–α12 and β-strands β9–β11 form the C-terminal domain (Figs. 2*b* and 3). However, the arrangement of the two subunits of the enzyme was substantially different from that of *C. glutamicum* DAPDH. The two monomers that make up the *C. glutamicum* DAPDH dimer (PDB entry 1dap) are not identical. One subunit within the dimer (subunit *B*) contains NADP$^+$ and two acetic acid molecules in the active site and is in a closed conformation, whereas the other subunit (subunit *A*) contains NADP$^+$ but no acetic acid molecule and is in an open conformation (Scapin *et al.*, 1996) (Fig. 4). By contrast, the two monomers that make up *U. thermosphaericus* DAPDH were nearly identical, with a backbone r.m.s.d. of 0.075 Å (Fig. 4), and similar features were observed in the NADP$^+$/TES-bound structure (see below). When the dinucleotide-binding and dimerization domains of *U. thermosphaericus* DAPDH were superimposed on the equivalent domains of subunits *A* and *B* of PDB entry 1dap, the C-terminal domain of *U. thermosphaericus* DAPDH was situated between the corresponding domains of subunits *A* (domain angle of 37°) and *B* (domain angle of 22°), and the domain angle of the enzyme (32°) was similar to that of the *C. glutamicum* DAPDH–*meso*-DAP binary complex (domain angle of 31°; PDB entry 2dap; Fig. 4).

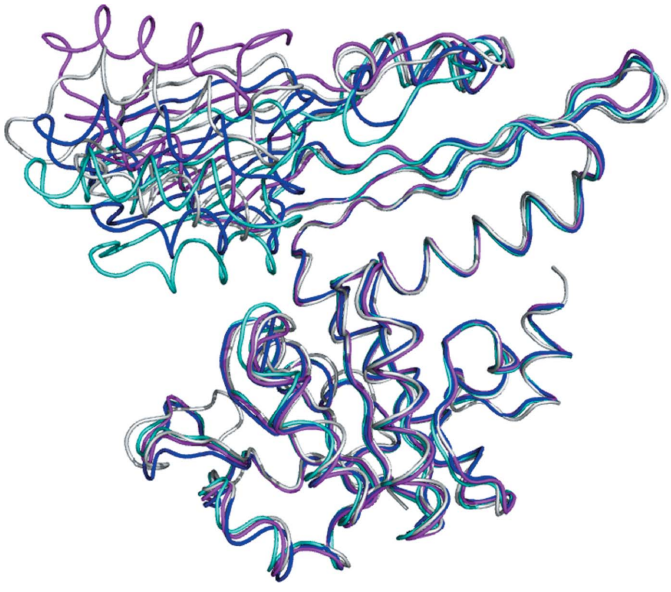

Figure 4
Comparison of the domain organization in the *C. glutamicum* and *U. thermosphaericus* DAPDH subunits. The dinucleotide-binding and dimerization domains of each subunit are superimposed. The open (subunit *A*) and closed (subunit *B*) conformations of the subunits of the *C. glutamicum* DAPDH dimer (PDB entry 1dap) are shown in magenta and cyan, respectively. The intermediate conformation of the subunit in the *C. glutamicum* DAPDH–*meso*-DAP binary complex (PDB entry 2dap) is shown in blue. The *U. thermosphaericus* DAPDH subunit is shown in grey.

The *U. thermosphaericus* DAPDH monomer also showed high structural similarity to DAPDH from *S. thermophilum* (PDB entries 3wb9, 3wbb and 3wbf, with r.m.s.d.s between 1.6 and 3.1 Å; Liu *et al.*, 2014), but α9 and α10 in the structure of the former were replaced by a short loop in the latter (Fig. 3). In addition, although the *S. thermophilum* enzyme assembled into a hexamer, a dimeric structure similar to the *U. thermosphaericus* and *C. glutamicum* DAPDHs was seen within the hexamer. Analysis of interfacing residues using *PISA*, followed by sequence alignment, indicated that the sequence similarity at the equivalent dimeric interface between *U. thermosphaericus* and *C. glutamicum* DAPDHs was 80% and that between *U. thermosphaericus* and *S. thermophilum* DAPDHs was 71%. On the other hand, superposition of the *U. thermosphaericus* DAPDH dimer onto the equivalent dimeric block of *S. thermophilum* DAPDH showed that α9 and α10 of the *U. thermosphaericus* enzyme would sterically hinder the binding of the other dimeric block of the *S. thermophilum* enzyme (data not shown). This may preclude hexamer formation for *U. thermosphaericus* DAPDH. Since the two helices are also conserved in *C. glutamicum* DAPDH, these elements are likely to contribute to the DAPDH dimer association. Structures of *S. thermophilum* DAPDH have been determined in the apo form (PDB entry 3wb9), in complex with NADP$^+$ (PDB entry 3wbb) and in complex with both NADPH and *meso*-DAP (PDB entry 3wbf). Upon substrate/cofactor binding, domain movement similar to that seen in *C. glutamicum* DAPDH was also observed in *S. thermophilum* DAPDH. In all cases, however, the monomers that make up the hexamer were nearly identical, and each subunit exhibited the same binding mode for the substrate/cofactor.

3.2. NADP$^+$-bound DAPDH structure

The structure of NADP$^+$-bound DAPDH was determined at a resolution of 2.07 Å (PDB entry 3wyc; Table 1). The final model (a dimer) was composed of amino-acid residues 2–328 in each subunit (residue Arg328 was represented by Ala because of the poor electron density of the side chain), two NADP$^+$ coenzymes, four TES molecules and 387 water molecules. In the initial electron-density map of NADP$^+$-bound DAPDH an extra density within the active-site cavity

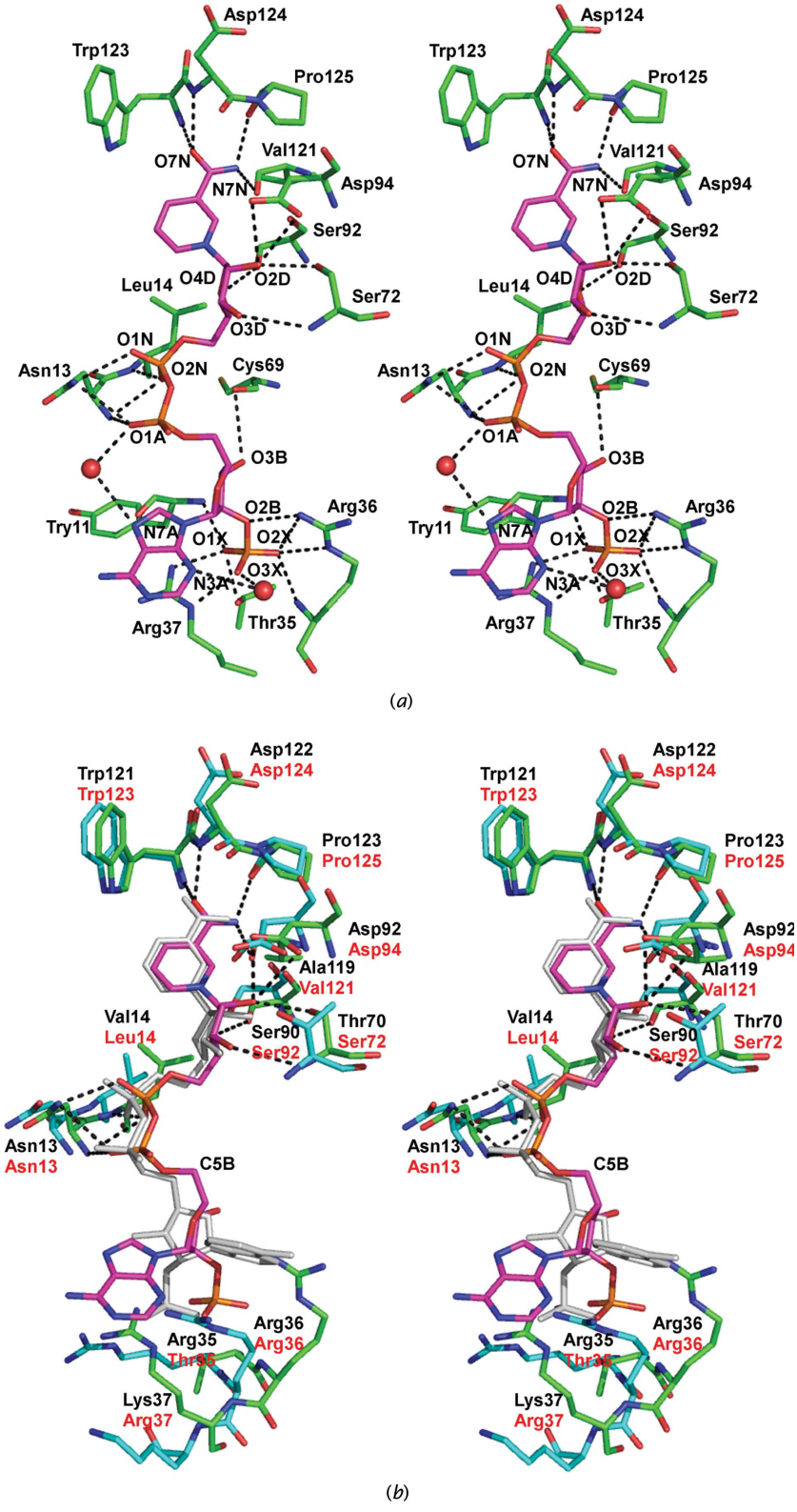

Figure 5
(*a*) Stereo representation of NADP$^+$ bound to *U. thermosphaericus* DAPDH. The NADP$^+$ molecule is shown in magenta. Water molecules are shown as red spheres. The networks of hydrogen bonds are shown as dotted lines. O and N atoms are shown in red and blue, respectively. (*b*) Comparison of NADP$^+$-binding sites in *U. thermosphaericus* DAPDH (green and red labels) and *S. thermophilum* DAPDH (cyan and black labels). NADP$^+$ molecules are shown in magenta and grey in the *U. thermosphaericus* and *S. thermophilum* enzymes, respectively.

was observed, and after construction and refinement of the peptide chain a TES molecule could be modelled into this density (Supplementary Fig. S1). In addition, another TES molecule was bound to the α3 and α4 helices (around the side chains of Asp54, Glu78, Gln79 and Tyr82 in both subunits; Supplementary Fig. S1). Although the enzyme was co-crystallized with D-lysine, a substrate analogue, electron density for a D-lysine molecule was not obtained.

The NADP$^+$ bound within the nucleotide-binding site is illustrated in Fig. 5(*a*). Four hydrogen-bond interactions are made between the nicotinamide amide group (O7N and N7N) and the backbone O atoms of Val121 and Pro125 and the backbone N atoms of Trp123 and Asp124. The C2 and C3 hydroxyl groups (O2D and O3D) of the nicotinamide ribose interact with the side chains of Asp94 and Ser72 and the backbone N atom of Ser72. The ribose O4D interacts with the side chain of Ser92. The nicotinamide phosphate (O1N and O2N) interacts with the backbone N atoms of Asn13 and Leu14 and the side chain of Asn13. The adenine phosphate (O1A) also interacts with the backbone N atom and side chain of Asn13. The C3 hydroxyl group (O3B) of the adenine ribose interacts with the backbone O atom of Cys69. The C2 phosphate group (O1X, O2X and O3X) of the adenine ribose interacts with the side chains of Thr35, Arg36 and Arg37 and the backbone N atoms of Arg36 and Tyr11, while the O atom (O2B) linking the phosphate to the nucleotide forms a hydrogen bond to the side chain of Arg36. *Via* water molecules, N3A and N7A of the adenine base interact with the C2 phosphate group of the adenine ribose and the adenine phosphate, respectively. Most of the summarized interactions are conserved in the NADP$^+$-bound *C. glutamicum* DAPDH structure, although Thr35, Ser92 and Val121 in *U. thermosphaericus* DAPDH are replaced by Ser35, Thr88 and Thr117, respectively, in *C. glutamicum* DAPDH. The NADP$^+$ molecule in *U. thermosphaericus* DAPDH is thus positioned/configured in a similar fashion to that in *C. glutamicum* DAPDH. On the other hand, when the NADP$^+$-bound *S. thermophilum* DAPDH structure was superimposed on the structure of NADP$^+$-bound *U. thermosphaericus* DAPDH, the mode of cofactor binding differed between the two enzymes (Fig. 5*b*). The interactions between the nicotinamide, nicotinamide ribose and pyrophosphate moiety of NADP$^+$ and the enzyme are similar in the two enzymes, but a remarkable structural

difference is found at the adenine and adenine ribose moieties. In *S. thermophilum* DAPDH, these moieties rotate in a clockwise direction around C5B of $NADP^+$ by about 80° relative to those in *U. thermosphaericus* DAPDH and are located in a much more solvent-exposed area. This occurs because the relative positions of the residues that interact with the C2 phosphate group of the adenine ribose differ greatly between the two enzymes: Thr35, Arg36 and Arg37 in *U. thermosphaericus* DAPDH are replaced by Arg35, Arg36 and Lys37, respectively, in *S. thermophilum* DAPDH (Fig. 5*b*).

When the structure of apo *U. thermosphaericus* DAPDH was superimposed on the structure of $NADP^+$/TES-bound *U. thermosphaericus* DAPDH, no substantive difference was observed between the two structures, which had a backbone r.m.s.d. of 0.33 Å. A structural change that occurs upon the binding of $NADP^+$ to the enzyme is the rotation of the side chains of Arg36 and Arg37 to form hydrogen-bonding interactions with the C2 phosphate group of the adenine ribose.

3.3. Insight into the C-terminal residue

As described above, one subunit of the dimeric *C. glutamicum* DAPDH is in an open conformation, while the other is in a closed, substrate-bound conformation. The open and closed conformations of the subunits are thought to represent the binding and active states of the enzyme, respectively, which may reflect an intrinsic 'half-of-the-sites' reactivity of the enzyme (Scapin *et al.*, 1996). The C-terminal tail (residues 300–320) in *C. glutamicum* DAPDH extends from one subunit into the other subunit. In the closed conformation, the carboxyl group of the C-terminal *Val320 forms hydrogen bonds to the side chains of Arg128 and His92, which derive from α5 in the dimerization domain and α4 in the dinucleotide-binding domain, respectively (the asterisk indicates a residue in the neighbouring subunit; Fig. 6*a*). The side chains of both Arg128 and His92 also

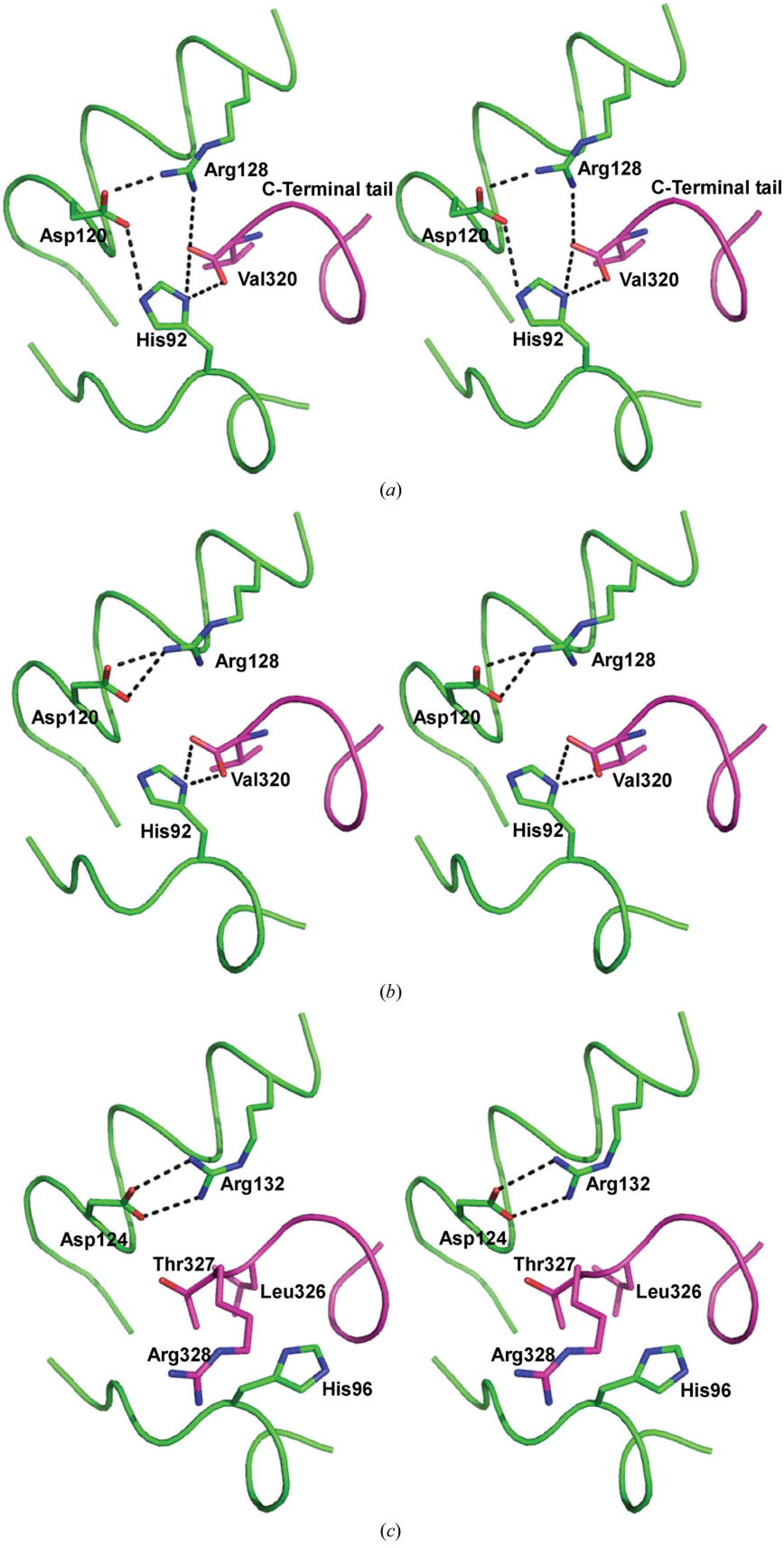

Figure 6
Stereographic close-up of the C-terminal region from the adjacent subunit. (*a*) *C. glutamicum* DAPDH subunit in the closed conformation, (*b*) *C. glutamicum* DAPDH subunit in the open conformation and (*c*) *U. thermosphaericus* DAPDH subunit. The C-terminal tail from the adjacent subunit is shown in magenta. The hydrogen bonds around the C-terminal residues are shown as dotted lines. Atoms are coloured as in Fig. 5(*a*).

Table 2
Comparison of the structural features of DAPDHs from *C. glutamicum*, *U. thermosphaericus* and *S. thermophilum*.

Enzyme (PDB entry)	*U. thermosphaericus* DAPDH (3wyc)	*C. glutamicum* DAPDH (1dap)	*S. thermophilum* DAPDH (3wbb)
Sequence identity (%)	—	46	33
R.m.s.d. (Å^2)	—	1.8	1.4
Assembly	Dimer	Dimer	Hexamer
ASA (Å^2)			
Oligomer	26800	25700	66900
Monomer	16700	15600	15400
Interface area (Å^2)	3200	2700	2700 (dimer) 12900 (hexamer)
No. of ion pairs			
Monomer	34 (subunit *A*) 32 (subunit *B*)	50 (subunit *A*) 53 (subunit *B*)	42 (subunits *A*, *D*) 39 (subunits *B*, *E*) 42 (subunits *D*, *F*)
Oligomer	66	103	246
Interface	8	2	13 (*AC* dimer) 8 (*BE* dimer) 13 (*DF* dimer) 46 (hexamer)
No. of hydrophobic interactions			
Monomer	446 (subunit *A*) 447 (subunit *B*)	357 (subunit *A*) 361 (subunits *B*)	358 (subunit *A*, *D*) 368 (subunits *B*, *E*) 360 (subunits *D*, *F*)
Oligomer	893	718	2172
Interface	159	49	112 (*AC* dimer) 116 (*BE* dimer) 112 (*DF* dimer) 467 (hexamer)
Content of accessible surface area			
Charged (%)	48	45	47
Polar (%)	30	26	19
Hydrophobic (%)	22	29	34
No. of amino-acid residues			
Total	326	320	229
Proline	16	14	17
Glycine	27	25	26

interact with the side chain of Asp120, which belongs to α5. In the open conformation, on the other hand, the carboxyl group of *Val320 only interacts with the side chain of His92 because the positioning of the Arg128 side chain is too far away to maintain the interaction (Fig. 6*b*). Likewise, the interaction between the side chains of His92 and Asp120 is also abolished in the open conformation. These observations suggest that the carboxyl group of the C-terminal *Val320 may be involved in stabilization of the closed conformation of *C. glutamicum* DAPDH. Arg128, His92 and Asp120 of *C. glutamicum* DAPDH are completely conserved in *U. thermosphaericus* DAPDH as Arg132, His96 and Asp124, respectively. In addition, the C-terminal tail (residues 306–328) also extends towards the corresponding region in the other subunit. However, the two C-terminal residues (Thr327 and Arg328) in *U. thermosphaericus* DAPDH, which are derived from the C-terminal His tag, sterically hinder access of the His96 side chain to *Leu326, the residue equivalent to the C-terminal *Val320 in *C. glutamicum* DAPDH (Fig. 6*c*).As a result, the side chain of His96 is situated such that it does not interact with Asp124 or *Leu326. It would therefore be of interest to test whether untagged *U. thermosphaericus* DAPDH undergoes conformational changes similar to *C. glutamicum* DAPDH.

In the case of *S. thermophilum* DAPDH, the three aforementioned residues and the C-terminal Val are conserved as Arg130, His94, Asp122 and Val299, respectively, and hydrogen-bonding interactions are observed among these residues. However, the replacement of these hydrogen bonds associated with substrate binding is not observed (data not shown). Thus, the unique hexameric arrangement of *S. thermophilum* DAPDH may be responsible for its distinctive substrate-recognition mechanism.

3.4. Structural features underlying thermostability

S. thermophilum DAPDH is the most thermostable DAPDH yet described; the enzyme retains more than 90% of its activity after heating at 343 K for 1 h (Gao *et al.*, 2012). By contrast, *C. glutamicum* DAPDH becomes completely inactive within 10 min at temperatures above 321 K (Misono *et al.*, 1986). *U. thermosphaericus* DAPDH also shows high thermostability, with no loss of activity after incubation for 30 min at 333 K, but is less thermostable than *S. thermophilum* DAPDH, as it loses 50% of activity after incubation for 30 min at 338 K (Akita *et al.*, 2011). A fluorescence-based thermal shift assay of *U. thermosphaericus* DAPDH showed that the enzyme has a T_m of around 336.5 K (Supplementary Fig. S2). In this assay, upon protein unfolding the exposed hydrophobic surfaces bind the SYPRO Orange dye, resulting in an increase in fluorescence (Lo *et al.*, 2004). This suggests that the loss of activity after incubation at 338 K is caused by protein unfolding and not just by catalytic site perturbation. Because the subunit assembly of *U. thermosphaericus* DAPDH (a dimer) is quite different from that of *S. thermophilum* DAPDH (a hexamer), the structural features responsible for their high thermostability were evaluated in comparison with the structure of *C. glutamicum* DAPDH.

Structural studies of thermophilic enzymes have suggested that the number of ion pairs and the formation of ion-pair networks contribute significantly to the thermostability of these enzymes (Hennig *et al.*, 1995; Yip *et al.*, 1995; Karshikoff & Ladenstein, 2001). Using a cutoff distance of 4.0 Å between oppositely charged residues, we calculated that the *C. glutamicum* DAPDH (PDB entry 1dap) monomer contained 50–53 intrasubunit ion pairs, whereas the *U. thermosphaericus* DAPDH (PDB entry 3wyc) monomer contained only 32–34 intrasubunit ion pairs (Table 2). Moreover, no major ion-pair network was observed in the *U. thermosphaericus* DAPDH monomer, although *C. glutamicum* DAPDH

contained three kinds of three-residue networks (Glu177–Arg180–Glu262, Glu310–Arg318–Asp319 and Lys20–Arg269–Asp272) in subunit *A* and four kinds of three-residue networks (Glu177–Arg180–Glu262, Glu310–Arg318–Asp319, Lys20–Arg269–Asp272 and Lys164–Glu232–Asp236) and one kind of four-residue network (Arg36–Asp71–Asp154–Arg158) in subunit *B*. Among the networks in subunit *B*, the Arg36–Asp71–Asp154–Arg158 network was located between the dinucleotide-binding and C-terminal domains and is likely to be involved in the conformational change of this subunit. On the other hand, two major intersubunit ion-pair networks between the *A* and *B* subunits were observed in *U. thermosphaericus* DAPDH: Lys316–Glu324–*Glu136 and *Lys316–*Glu324–Glu136 (the asterisks indicate the neighbouring subunit in the dimer). Consequently, the number of intersubunit ion pairs was markedly larger in *U. thermosphaericus* DAPDH (8) than *C. glutamicum* DAPDH (2) (Table 2).

Hydrophobic interactions are also known to participate in the stabilization of protein structures (Vieille & Zeikus, 2001; Bhuiya *et al.*, 2005). We found a striking difference in the number of intersubunit hydrophobic interactions between *U. thermosphaericus* DAPDH and *C. glutamicum* DAPDH: the former had a total of 159 intersubunit interactions, which was three times larger than in the latter (49) (Table 2). In this context, the intermolecular ASA of *U. thermosphaericus* DAPDH (3200 Å^2) was substantially larger than that of *C. glutamicum* DAPDH (2700 Å^2), although the total ASAs of the monomer and dimer were not so different between the two enzymes. Moreover, the total number of hydrophobic interactions within the *U. thermosphaericus* DAPDH monomer (446 in subunit *A* and 447 in subunit *B*) was much larger than that within *C. glutamicum* DAPDH (357 in subunit *A* and 361 in subunit *B*).

An increase in charged surface amino-acid residues and a corresponding decrease in polar and/or hydrophobic surface content have been shown to contribute to greater protein thermostability (Fukuchi & Nishikawa, 2001). As shown in Table 2, the content of charged surface residues in *U. thermosphaericus* DAPDH (48%) was comparable to that in *C. glutamicum* DAPDH (45%), although a decrease in the hydrophobic surface content was observed in the former. Increased backbone rigidity is also known to be an important factor for the stabilization of protein structures (Závodszky *et al.*, 1998). The presence of a glycine residue allows backbone flexibility in this region, whereas proline residues lock the backbone into a limited conformation. The total number of glycine or proline residues in *U. thermosphaericus* DAPDH was similar to that in *C. glutamicum* DAPDH (Table 2). Overall, these results indicate that the presence of large numbers of intrasubunit and intersubunit hydrophobic interactions, as well as the extensive formation of intersubunit ion-pair networks, are likely to be the main factors contributing to the high thermostability of *U. thermosphaericus* DAPDH.

On the other hand, the total ASA of the *S. thermophilum* DAPDH monomer (15 400 Å^2) was similar to that of the *C. glutamicum* enzyme monomer (15 600 Å^2), and we found no significant difference in the number of hydrophobic interactions per monomer between the two enzymes. In addition, the number of ion pairs within the monomeric *S. thermophilum* structure (39–42) was also less than in *C. glutamicum* DAPDH. The *S. thermophilum* DAPDH monomer contained one ion-pair network of three residues (Arg165–Glu186–Glu188) and one ion-pair network of four residues (Glu232–Arg246–Glu248–Arg250) in subunits *A*, *C*, *D* and *F*, and two ion-pair networks of three residues (Arg165–Glu186–Glu188 and Lys180–Glu210–Arg212) and one ion-pair network of four residues (Glu232–Arg246–Glu248–Arg250) in subunits *B* and *E*. Thus, the scale of the ion-pair networks per monomer in *S. thermophilum* DAPDH was comparable to that in the *C. glutamicum* enzyme. When we compared the intersubunit interactions in *U. thermosphaericus* DAPDH with those in a corresponding dimer of *S. thermophilum* DAPDH, we found that the number of hydrophobic interactions in the former (159) was markedly larger than that in the latter (112–116). By contrast, large intersubunit ion-pair networks were observed in a corresponding dimer of *S. thermophilum* DAPDH, although the number of ion pairs was not largely different between the two enzymes (8 *versus* 8–13). Two ion-pair networks of seven residues (*Asp99–*Arg101–*Glu280–Asp285–Arg291–Glu292–Arg296 and Asp99–Arg101–Glu280–*Asp285–*Arg291–*Glu292–*Arg296) were located between subunits *B* and *E*, and four networks of four residues (*Asp99–*Arg102–Glu292–Arg296, *Arg101–*Glu280–Asp285–Arg291, Asp99–Arg102–*Glu292–*Arg296 and Arg101–Glu280–*Asp285–*Arg291) were located

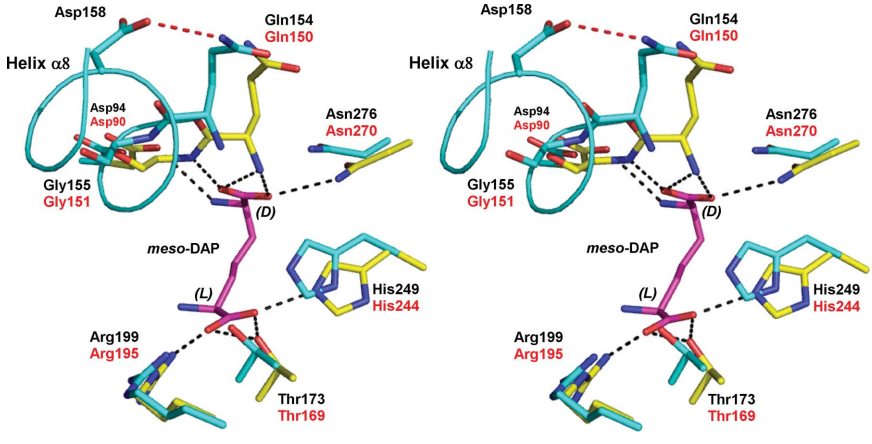

Figure 7
Stereographic close-up of the substrate-binding site in *U. thermosphaericus* DAPDH. The structure of *C. glutamicum* DAPDH (PDB entry 2dap; yellow and red labels) is superimposed on that of *U. thermosphaericus* DAPDH (cyan and black labels). A *meso*-DAP molecule bound to *C. glutamicum* DAPDH is shown as a stick model in magenta. The hydrogen bond between Asp158 and Gln154 in *U. thermosphaericus* DAPDH is shown as a dashed red line. The networks of hydrogen bonds in *C. glutamicum* DAPDH are shown as dashed black lines. Atoms are coloured as in Fig. 4.

between subunits *A* (*D*) and *C* (*F*) (the asterisks indicate the neighbouring subunit in the dimer). Furthermore, as a result of the hexameric assembly of *S. thermophilum* DAPDH, the total number of intersubunit interactions was calculated to be huge for both ion-pair (46) and hydrophobic (467) interactions. The content of charged surface residues and the total number of glycine or proline residues in *S. thermophilum* DAPDH were similar to those of the other two enzymes (Table 2).

A few enzymes from thermophiles have been reported to assume a higher oligomerization state than their mesophilic counterparts. These include *Thermococcus kodakaraensis* KOD1 ribulose 1,5-bisphosphate carboxylase/oxygenase (Maeda *et al.*, 2002) and *Aeropyrum pernix* 2-deoxy-D-ribose-5-phosphate aldolase (Sakuraba *et al.*, 2003). The unique hexameric assembly of *S. thermophilum* DAPDH, as well as the formation of the large intersubunit ion-pair networks, may thus contribute to its high thermostability. Our observation suggests that the molecular strategy for increasing thermostability substantially differs between *S. thermophilum* DAPDH and *U. thermosphaericus* DAPDH.

3.5. Insight into substrate-recognition mechanism

We have already been able to create a stable DAADH from *U. thermosphaericus* DAPDH by introducing five point mutations, Gln154Leu, Asp158Gly, Thr173Ile, Arg199Met and His249Asn (Akita *et al.*, 2012*a*,*b*), in a manner similar to that used to create the *C. glutamicum* DAADH (Vedha-Peters *et al.*, 2006). The *U. thermosphaericus* DAADH does not act on *meso*-DAP (Akita *et al.*, 2012*a*,*b*) and differs greatly from the parent DAPDH, which acts exclusively on *meso*-DAP as the specific electron donor (Akita *et al.*, 2011). In addition, this DAADH catalyzes the reversible deamination of D-amino acids such as D-cyclohexylalanine (relative activity 100%), D-isoleucine (73%), D-2-aminooctanoate (61%) and D-lysine (53%) (Akita *et al.*, 2012*a*,*b*). To assess the difference in the substrate-recognition mechanism between DAPDH and DAADH, the active-site architecture of *U. thermosphaericus* DAPDH was compared with that of *C. glutamicum* DAPDH.

The crystal structure of the *C. glutamicum* DAPDH–*meso*-DAP binary complex has been reported (Scapin *et al.*, 1998). Superposition of this structure (PDB entry 2dap) onto that of $NADP^+$/TES-bound *U. thermosphaericus* DAPDH enabled comparison of the amino-acid residues involved in substrate binding (Fig. 7). Within the structure of the *C. glutamicum* DAPDH–*meso*-DAP complex, the α-carboxylate of the D-amino-acid centre of *meso*-DAP forms four hydrogen bonds to the main-chain N atoms of Gln150 and Gly151 and the side chain of Asn270, while the α-amino group of the D-amino-acid centre forms one hydrogen bond to the side chain of Asp90. On the other hand, the α-carboxylate of the L-amino-acid centre of *meso*-DAP forms four hydrogen bonds to the side chains of Arg195, Thr169 and His244, and no hydrogen-bonding interactions are observed between the α-amino group of the L-amino-acid centre and the enzyme. The residues that interact with *meso*-DAP in *C. glutamicum* DAPDH (Asp90, Gln150, Gly151, Thr169, Arg195, His244 and Asn270) are completely conserved in *U. thermosphaericus* DAPDH as Asp94, Gln154, Gly155, Thr173, Arg199, His249 and Asn276, respectively (Fig. 7). Among these residues, Gln154, Thr173, Arg199 and His249 are replaced by Leu, Ile, Met and Asn, respectively, in DAADH. Although Gln154 is replaced by Leu, the hydrogen-bonding interactions around the D-amino-acid centre of *meso*-DAP would be conserved in DAADH because the backbone amide of the Leu is thought to be situated in a position where it can interact with the α-carboxylate of the D-amino-acid centre, as Gln154 does. By contrast, most of the hydrogen-bonding interactions around the L-amino-acid centre might be lost in DAADH because Thr173 and Arg199 in DAPDH, the side chains of which make hydrogen bonds to the α-carboxylate of the L-amino-acid centre, are replaced by Ile and Met, respectively. These observations suggest that the loss of interactions between the L-amino-acid centre of *meso*-DAP and the enzyme is likely to be responsible for the lack of reactivity of DAADH towards *meso*-DAP. Conversely, the Thr173Ile and Arg199Met substitutions may enhance the hydrophobicity of the pocket around the L-amino-acid centre, and this appears to be related to the high reactivity of DAADH for the hydrophobic D-amino acids, including D-cyclohexylalanine, D-isoleucine and D-2-aminooctanoate.

In *U. thermosphaericus* DAPDH, on the other hand, the side chain of Asp158, which belongs to helix α8, forms a hydrogen bond to the side chain of Gln154, the N-terminal residue of helix α8 (Fig. 7). The Gln154Leu and Asp158Gly mutations abolish this interaction and appear to enhance the flexibility of the α8 N-terminal residues that interact with the D-amino-acid centre of the substrate. This may explain the enlarged substrate range in *U. thermosphaericus* DAADH, because substitution of Asp154Gly in *C. glutamicum* DAADH, which corresponds to Asp158Gly in the *U. thermosphaericus* enzyme, reportedly also enhances the reactivity toward a broad range of substrates (Vedha-Peters *et al.*, 2006). At the present time, however, the details of the substrate-recognition mechanism of DAADH are still unclear. The structure of the *U. thermosphaericus* DAADH–cofactor–substrate ternary complex should be a useful focus for further investigation.

Acknowledgements

We are grateful to all of the laboratory members at Kagawa University and Kyushu University for their technical assistance and valuable discussions. This work was supported by grants from KAKENHI (25·4653 to HA and 22248010 to TO). This work was also supported by a grant for the Promotion of Basic Research Activities for Innovative Bioscience from the Bio-oriented Technology Research Advancement Institution (BRAIN).

References

Akita, H., Doi, K., Kawarabayasi, Y. & Ohshima, T. (2012*a*). *Biotechnol. Lett.* **34**, 1693–1699.

Akita, H., Doi, K., Kawarabayasi, Y. & Ohshima, T. (2012*b*). *Biotechnol. Lett.* **34**, 1701–1702.

Akita, H., Fujino, Y., Doi, K. & Ohshima, T. (2011). *AMB Express*, **1**, 43.

Akita, H., Imaizumi, Y., Suzuki, H., Doi, K. & Ohshima, T. (2014). *Biotechnol. Lett.* **36**, 2245–2248.

Akita, H., Suzuki, H., Doi, K. & Ohshima, T. (2014). *Appl. Microbiol. Biotechnol.* **98**, 1135–1143.

Bhuiya, M. W., Sakuraba, H., Ohshima, T., Imagawa, T., Katunuma, N. & Tsuge, H. (2005). *J. Mol. Biol.* **345**, 325–337.

Bradford, M. M. (1976). *Anal. Biochem.* **72**, 248–254.

Brünger, A. T., Adams, P. D., Clore, G. M., DeLano, W. L., Gros, P., Grosse-Kunstleve, R. W., Jiang, J.-S., Kuszewski, J., Nilges, M., Pannu, N. S., Read, R. J., Rice, L. M., Simonson, T. & Warren, G. L. (1998). *Acta Cryst.* D**54**, 905–921.

Cirilli, M., Scapin, G., Sutherland, A., Vederas, J. C. & Blanchard, J. S. (2000). *Protein Sci.* **9**, 2034–2037.

Cowtan, K. D. & Main, P. (1996). *Acta Cryst.* D**52**, 43–48.

Emsley, P., Lohkamp, B., Scott, W. G. & Cowtan, K. (2010). *Acta Cryst.* D**66**, 486–501.

Fukuchi, S. & Nishikawa, K. (2001). *J. Mol. Biol.* **309**, 835–843.

Gao, X., Chen, X., Liu, W., Feng, J., Wu, Q., Hua, L. & Zhu, D. (2012). *Appl. Environ. Microbiol.* **78**, 8595–8600.

Gao, X., Huang, F., Feng, J., Chen, X., Zhang, H., Wang, Z., Wu, Q. & Zhu, D. (2013). *Appl. Environ. Microbiol.* **79**, 5078–5081.

Hennig, M., Darimont, B., Sterner, R., Kirschner, K. & Jansonius, J. N. (1995). *Structure*, **3**, 1295–1306.

Holm, L. & Rosenström, P. (2010). *Nucleic Acids Res.* **38**, W545–W549.

Karshikoff, A. & Ladenstein, R. (2001). *Trends Biochem. Sci.* **26**, 550–556.

Krissinel, E. & Henrick, K. (2007). *J. Mol. Biol.* **372**, 774–797.

Liu, W., Li, Z., Huang, C.-H., Guo, R.-T., Zhao, L., Zhang, D., Chen, X., Wu, Q. & Zhu, D. (2014). *Chembiochem*, **15**, 217–222.

Lo, M.-C., Aulabaugh, A., Jin, G., Cowling, R., Bard, J., Malamas, M. & Ellestad, G. (2004). *Anal. Biochem.* **332**, 153–159.

Lovell, S. C., Davis, I. W., Arendall, W. B. III, de Bakker, P. I., Word, J. M., Prisant, M. G., Richardson, J. S. & Richardson, D. C. (2003). *Proteins*, **50**, 437–450.

Maeda, N., Kanai, T., Atomi, H. & Imanaka, T. (2002). *J. Biol. Chem.* **277**, 31656–31662.

Matthews, B. W. (1968). *J. Mol. Biol.* **33**, 491–497.

McNicholas, S., Potterton, E., Wilson, K. S. & Noble, M. E. M. (2011). *Acta Cryst.* D**67**, 386–394.

Misono, H., Ogasawara, M. & Nagasaki, S. (1986). *Agric. Biol. Chem.* **50**, 2729–2734.

Misono, H. & Soda, K. (1980). *J. Biol. Chem.* **255**, 10599–10605.

Misono, H., Togawa, H., Yamamoto, T. & Soda, K. (1979). *J. Bacteriol.* **137**, 22–27.

Murshudov, G. N., Skubák, P., Lebedev, A. A., Pannu, N. S., Steiner, R. A., Nicholls, R. A., Winn, M. D., Long, F. & Vagin, A. A. (2011). *Acta Cryst.* D**67**, 355–367.

Otwinowski, Z. & Minor, W. (1997). *Methods Enzymol.* **276**, 307–326.

Rodriguez, R., Chinea, G., Lopez, N., Pons, T. & Vriend, G. (1998). *Bioinformatics*, **14**, 523–528.

Sakuraba, H., Tsuge, H., Shimoya, I., Kawakami, R., Goda, S., Kawarabayasi, Y., Katunuma, N., Ago, H., Miyano, M. & Ohshima, T. (2003). *J. Biol. Chem.* **278**, 10799–10806.

Scapin, G., Cirilli, M., Reddy, S. G., Gao, Y., Vederas, J. C. & Blanchard, J. S. (1998). *Biochemistry*, **37**, 3278–3285.

Scapin, G., Reddy, S. G. & Blanchard, J. S. (1996). *Biochemistry*, **35**, 13540–13551.

Thompson, J. D., Higgins, D. G. & Gibson, T. J. (1994). *Nucleic Acids Res.* **22**, 4673–4680.

Vagin, A. & Teplyakov, A. (2010). *Acta Cryst.* D**66**, 22–25.

Vedha-Peters, K., Gunawardana, M., Rozzell, J. D. & Novick, S. J. (2006). *J. Am. Chem. Soc.* **128**, 10923–10929.

Vieille, C. & Zeikus, G. J. (2001). *Microbiol. Mol. Biol. Rev.* **65**, 1–43.

Watanabe, M., Inoue, H., Inoue, B., Yoshimi, M., Fujii, T. & Ishikawa, K. (2014). *AMB Express*, **4**, 27.

Winn, M. D. *et al.* (2011). *Acta Cryst.* D**67**, 235–242.

Yip, K. S. P., Stillman, T. J., Britton, K. L., Artymiuk, P. J., Baker, P. J., Sedelnikova, S. E., Engel, P. C., Pasquo, A., Chiaraluce, R., Consalvi, V., Scandurra, R. & Rice, D. W. (1995). *Structure*, **3**, 1147–1158.

Závodszky, P., Kardos, J., Svingor, Á. & Petsko, G. A. (1998). *Proc. Natl Acad. Sci. USA*, **95**, 7406–7411.